TASI Lectures on Jet Substructure

Jessie Shelton[*]

Yale University Physics Department and
Harvard University Physics Department
High Energy Theory Group
17 Oxford Street
Cambridge, MA 02138, USA

June, 2012

Abstract

Jet physics is a rich and rapidly evolving field, with many applications to physics in and beyond the Standard Model. These notes, based on lectures delivered at the June 2012 Theoretical Advanced Study Institute, provide an introduction to jets at the Large Hadron Collider. Topics covered include sequential jet algorithms, jet shapes, jet grooming, and boosted Higgs and top tagging.

---

[*]jshelton@physics.harvard.edu

Contents

1 Introduction

These notes are writeups of three lectures delivered at the Theoretical Advanced Study Institute in Boulder, Colorado, in June 2012. The aim of the lectures is to provide students who have little or no experience with jets with the basic concepts and tools needed to engage with the rapidly developing ideas concerning the use of jets in new physics searches at the LHC. A certain amount of familiarity with the structure of QCD, and in particular with QCD showers, is assumed.

Lecture one introduces sequential jet algorithms, and develops several main tools in substructure analyses using the boosted Higgs as an example. Lecture two delves further

into jet grooming and jet shapes, and in lecture three we conclude with an overview of top tagging and BSM searches.

2 Lecture I: Jets, Subjets, and Sequential Jet Algorithms

To understand jet substructure and its applications, we must first begin by understanding jets. Jets, together with parton distribution functions and factorization theorems, are the phenomenological tool that allow us to separate out the perturbatively describable hard interactions in proton-proton collisions, and thereby enable us to make quantitative predictions for events involving strongly interacting particles. Jet cross-sections necessarily depend on the algorithm used to define a jet. There are many jet algorithms, each one with its own strengths and weaknesses.

The first jet algorithm was developed for $e^+e^- \rightarrow$ hadron events by Sterman and Weinberg in 1977 [1]. In this algorithm events are declared to have two jets if all but a fraction ϵ of the total energy in the event can be contained within two cones of half-angle δ. That is, radiation off of one of the initial partons must be sufficiently hard,

$$E_{rad} > \epsilon \tag{2.1}$$

and at sufficiently wide angles from either of the other jets,

$$\theta_{min} > \delta \tag{2.2}$$

for the radiation to be resolved as a separate jet. How many events have two jets and how many contain three or more obviously depends on the exact values chosen for ϵ and δ. For all sufficiently large ϵ/E_{tot} and δ, the partonic cross-section for radiation of an extra parton into the region of phase space defined by Eqs. 2.1 and 2.2 is sufficiently isolated from the soft and collinear singular regions of phase space that rates and distributions can be calculated reliably in perturbation theory. Of course, this is a partonic calculation, and to fully match the partonic picture onto reconstructed sprays of hadrons requires some additional theoretical machinery to describe such effects as (for example) hadronization. For our purposes, however, a parton shower picture will suffice.

The Sterman-Weinberg algorithm is the ur-example of a *cone* algorithm. While cone algorithms present a very intuitive picture of parton radiation, they can be somewhat clumsy in practice, particularly as the number of jets increases, and they are not in active

use in most experiments today. Other algorithms can deal much more flexibly with high jet multiplicity. One such flexible algorithm is the JADE algorithm, developed by the JADE collaboration in the late 1980s, also for $e^+e^- \to$ hadrons [2, 3]. Here, jets are constructed by iteratively recombining final state particles. Define a metric to measure the separation between final state particles i and j,

$$y_{ij} \equiv \frac{m_{ij}^2}{Q^2} \approx \frac{2E_iE_j(1 - \cos^2\theta_{ij})}{Q^2}, \tag{2.3}$$

where Q is the total energy of the event. Note that y_{ij} vanishes if either i or j is soft ($E_i \to 0$ or $E_j \to 0$), or if i and j are collinear ($\cos\theta_{ij} \to 1$). We can now construct jets using the following recipe:

- Compute the interparticle distances y_{ij} for all particles in the final state, and find the pair $\{i, j\}$ with the minimum y_{ij}.

- If this minimum $y_{ij} < y_0$ for some fixed parameter y_0, combine i and j into a new particle, and go back to the previous step.

- If $y_{ij} > y_0$, declare all remaining particles to be jets.

Since clustering of particles proceeds from smaller values of y_{ij} to larger values, this recipe preferentially clusters particles that are probing the regions of phase space dominated by the soft and collinear singularities. In a sense, the algorithm is trying to combine hadrons into partons by making its best guess for the reconstructed parton shower. The JADE algorithm has only one parameter, the separation cutoff y_0, and clearly can handle different jet multiplicities in an efficient way by varying y_0. It is the ur-example of a *sequential recombination algorithm*, and the ancestor of all jet algorithms in wide use at the LHC.

The most direct descendent of the JADE algorithm is the k_T *algorithm* [4], which replaces the particle energy factor E_iE_j in the Jade metric, Eq. 2.3, with the factor $\min(E_i^2, E_j^2)$:

$$y_{ij} = \frac{2\min(E_i^2, E_j^2)(1 - \cos^2\theta_{ij})}{Q^2}. \tag{2.4}$$

This still ensures that the metric goes to zero when either $E_i \to 0$ or $E_j \to 0$ are soft, but has the advantage that the relative softness of a particle depends only on its own energy, and not that of the other particle in the pair. This fixes up a technical drawback to the JADE algorithm, where $y_{ij}^{(JADE)} \propto E_iE_j$ allows two very soft particles to be combined even if they are at very wide angles from each other. Using $y_{ij} \propto \min(E_i^2, E_j^2)$ means soft particles will get preferentially clustered with nearby harder particles instead.

For small θ_{ij}, the numerator of Eq. 2.4 can be written as simply $k_\perp^2$, the transverse momentum of the softer particle relative to the harder particle—hence the name of the algorithm. In this form the metric is directly related to QCD splitting functions.

To create a version of the k_T algorithm that can be used at hadron colliders, where the total energy Q^2 is unknown, both the algorithm and the metric have to be adapted [5]. In the metric, we simply use longitudinally boost-invariant quantities p_T and ΔR instead of E and $\cos\theta_{ij}$, and let the metric become dimensionful,

$$d_{ij} = \frac{\min(p_{T,i}^2, p_{T,j}^2)\Delta R_{ij}^2}{R^2}. \tag{2.5}$$

The angular parameter R introduced here will replace y_0 as determining the cutoff for combining particles, as we will see. We need in addition to define the quantities

$$d_{iB} = p_{T,i}^2 \tag{2.6}$$

for each particle i, since we need to also consider splittings from the beam.

The recombination algorithm now works as follows:

- Compute d_{ij} and d_{iB} for all particles in the final state, and find the minimum value.

- If the minimum is a d_{iB}, declare particle i a jet, remove it from the list, and go back to step one.

- If the minimum is a d_{ij}, combine particles i and j, and go back to step one.

- Iterate until all particles have been declared jets.

This algorithm is usually what is meant by when the k_T algorithm is referred to, but you may occasionally see it referred to as the *inclusive k_T* algorithm, as there is a related (*"exclusive"*) variant [6]. Note that the parameter R functions as an angular cut-off: two particles separated by a distance $R_{ij} > R$ will never be combined, regardless of the p_T's of the particles (this does not necessarily preclude both particles being clustered into the same jet later). In fact, with this jet algorithm, arbitrarily soft particles can become jets. Therefore jets are customarily returned down to some finite p_T cutoff, typically tens of GeV.

Because the k_T algorithm clusters particles beginning with soft particles and working its way up to harder particles, the algorithm tends to construct irregular jets which depend on the detailed distribution of soft particles in an event. For this reason, k_T jets

are not especially practical for hadron colliders: irregular jets are hard to calibrate, and the jets are quite sensitive to unrelated radiation in the event.

Other sequential algorithms are obtained by using different metrics. The *Cambridge-Aachen* or C-A algorithm is obtained by taking [7]

$$d_{ij} = \frac{\Delta R_{ij}^2}{R^2}, \qquad d_{iB} = 1. \tag{2.7}$$

This metric clusters particles based only on their angular separation, giving a nicely geometric interpretation of jets. The C-A algorithm still reflects aspects of the QCD parton shower, in particular the *angular ordering* of emissions. However, it is less directly related to the structure of QCD parton splitting functions than the k_T algorithm is, and represents a compromise between reflecting the structure of the parton shower and maintaining some insensitivity to soft radiation.

The *anti-k_T* algorithm entirely abandons the idea of mimicking the parton shower [8]. Here, the metric is

$$d_{ij} = \min\left(\frac{1}{p_{T,i}^2}, \frac{1}{p_{T,j}^2}\right) \frac{\Delta R_{ij}^2}{R^2}, \qquad d_{iB} = \frac{1}{p_{T,i}^2}. \tag{2.8}$$

With this metric, particles are clustered beginning with the *hardest* particles. This means that the most energetic cores of jets are found first. As soft particles clustered later have a minimal impact on the larger four-momentum of the jet core, the anti-k_T algorithm tends to cluster particles out to distances R from the core of a jet, yielding very regular jets. Anti-k_T jets are therefore much easier to calibrate at experiments, and the anti-k_T algorithm has become the default used at the LHC.

Let us conclude this section by emphasizing that all sequential jet algorithms return not only a list of jets but a *clustering sequence* for the event. Varying the radial parameter R simply acts to move the resolution scale up and down the clustering sequence, making it very easy to study how jet distributions and multiplicities depend on the angular resolution R. In particular, for the C-A algorithm, the cluster sequence regarded as a function of R has a purely geometric interpretation as resolving the event on different angular scales.

All three sequential jet algorithms discussed here also share the same *reach*, that is, regardless of the chosen metric, a splitting $P \to ij$ will not be combined if the angular distance between the daughters exceeds the chosen jet radius, $\Delta R_{ij} > R$. This means that, to leading order, perturbative computations of quantities such as jet rates are identical between all three algorithms.

Finally, the infrared and collinear safety of all three sequential jet algorithms can be easily checked by asking how the cluster sequence would change with the addition of a soft or collinear emission. For the shower-sensitive k_T and C-A metrics, infrared and collinear safety follows automatically. The anti-k_T metric is also manifestly IR- and collinear-safe, as can be seen with a little more thought: anti-k_T recombinations are clearly collinear-safe, since collinear splittings are combined near the beginning of the sequence. IR safety also follows, as soft radiation has negligible impact on the jet built out from the hard core.

2.1   Jets at the LHC

The main subject of these lectures are the possibilities and uses of jets to discover physics at and beyond the electroweak scale, which means, for practical purposes, at the LHC.

It is important to remember that events at LHC are a busy hadronic environment. In addition to the showering and hadronizing hard partons which we want to study, there are large amounts of soft, unassociated radiation from (1) the *underlying event*, that is, the remnants of the scattering protons; (2) possible *multiple interactions*, that is, additional collisions of partons arising from the same *p-p* collision as the hard interaction; and (3) *pile-up*, additional *p-p* collisions from other protons in the colliding bunches. These additional sources of radiation contribute a potentially sizable and largely uniform backdrop of hadronic activity that, when clustered into jets, will partially obscure the features of the hard interaction that we would like to reconstruct.

The default jets used at the LHC are formed using the anti-k_T algorithm, with cone sizes $R = 0.4, 0.6$ (at ATLAS) and $R = 0.5, 0.7$ (at CMS). These specific choices of R come from a compromise between (1) the desire to collect all the radiation from a single parton, and (2) the desire *not* to sweep up an excessive amount of unrelated radiation.

Many advances have combined to make jets at the LHC a particularly fertile field.

- *advances in experiment*: the calorimeters at ATLAS and CMS have much finer resolution than in previous experiments, allowing a much more finely grained picture of events. Moreover, *local* calibration of jets allows jets to be considered on multiple scales.

- *advances in computation*: the development of fast algorithms [9] allows broad implementation of sequential recombination.

- *advances in energy*: the LHC center of mass energy is large enough that particles with weak scale masses (i.e., Z, W, t, and H) will for the first time have

an appreciable cross-section to be produced with enough of a boost to collimate the daughter partons. The simple picture that one parton corresponds to one jet breaks down badly in this case, and new tools are needed to separate out collimated perturbative decays from QCD showers.

There are several reasons to be interested in boosted particles. Very often, there is theoretical motivation to focus on a particular slice of phase space where the daughter particles are necessarily boosted. High mass resonances are the simplest such examples. For instance, a resonance ρ_C with mass $m_\rho \gtrsim 1.5$ TeV which decays to pairs of gauge bosons would yield highly boosted VV pairs.

Even in the absence of a resonance or other mechanism to preferentially populate boosted regions of phase space, looking for boosted signals can also be useful for improving the signal to background ratio. Changing the reconstruction method changes what the experimental definition of the signal is, and therefore necessarily the backgrounds change as well. This can sometimes—but not always!—be enough of an advantage to make up for the reduction in signal rate that comes from selecting only the boosted region of phase space. Background reduction comes in two forms. In high multiplicity final states, combinatoric background is often prohibitive. When some or all of the final state particles are boosted, the combinatoric background is greatly reduced. But it is also possible to use boosted selection techniques to identify regions where the background from other physics processes is intrinsically reduced.

To appreciate the need for new reconstruction techniques at the LHC, consider the production of top quarks at fixed center of mass energy $\sqrt{\hat{s}}$. Choosing some angular scale R_0, we can ask, what fraction of top quarks have all three, only two, or none of their partonic daughters isolated from the others at the scale R_0? This gives a zeroth order estimate of how well a jet algorithm with $R = R_0$ will be able to reconstruct the three partonic top daughters as separate jets. The answer we get depends sensitively on both R_0 and $\sqrt{\hat{s}}$:

$\sqrt{\hat{s}}$	R_0	3	2	1
1.5 TeV	0.4	0.55	0.45	—
1.5 TeV	0.6	0.2	0.6	0.2
2.0 TeV	0.6	0.1	0.45	0.45

Table 1: Resolved parton multiplicities in $t\bar{t}$ events

Clearly, tops produced in the very interesting super-TeV regime $\sqrt{\hat{s}} \gtrsim$ TeV straddle

the borderlines between several different topologies. It would be much more desirable to have a flexible reconstruction method that could handle semi-collimated tops in a unified way.

To see how we can go about building such reconstruction techniques, let's start by considering one of the landmark jet substructure analyses: the case of a boosted Higgs decaying into $b\bar{b}$.

2.2   Boosted Higgs

This analysis will introduce us to several ideas that will be important tools in our boosted analysis toolbox: fat jets, jet mass, jet grooming, and sequential de-clustering.

Searching for the Higgs in its decay to $b\bar{b}$ is very difficult at the LHC, due to overwhelming QCD backgrounds. Even in associated production, $pp \rightarrow HZ, HW$, the background processes $Z + b\bar{b}$, $W + b\bar{b}$, and even $t\bar{t}$ are overwhelming. Nonetheless, thanks to Ref. [10], $pp \rightarrow HV$, $H \rightarrow b\bar{b}$ is now an active search channel at the LHC.

To be specific, let's consider the process $pp \rightarrow HZ$, followed by $H \rightarrow b\bar{b}$, and $Z \rightarrow \ell^+\ell^-$. The traditional approach to this signal would be to look for final states with a leptonic Z and 2 b-tagged jets, construct the invariant mass of the jets, and look for a peak in the distribution of $m_{b\bar{b}}$. The new approach is instead to focus on events where the Higgs is produced with substantial p_T, $p_{T,H} > 200$ GeV, and cluster these events with a large ($R = 1.2$) jet radius, such that all of the Higgs decay products are swept up in a single fat jet. The signal is now a leptonic Z + a fat "Higgs-like" jet, and the background to this signal is now $Z+$ one fat jet rather than $Z + b\bar{b}$. What we'll see is that jet substructure offers us enough quantitative precision in what we mean by a "Higgs-like" jet to reduce the background by an extent that makes up for the acceptance price demanded by the high p_T cut.

For an unboosted search, the ultimate discriminator between signal and background is the b-$\bar{b}$ invariant mass: to find a resonance, look for a bump in the b-$\bar{b}$ mass spectrum. Now that we have boosted the Higgs and collected it into a single fat jet, the Higgs mass should be reflected in the invariant mass of the fat jet itself. To understand jet masses for the background, let's take a quick look at how jet masses are generated in QCD.

Jet Mass   . Partons are generally massless (we will neglect the b quark mass), but jets are not. Jet mass in QCD arises from emission during the parton shower, and as such we can calculate the leading contribution. Jet mass, like most perturbative jet properties in QCD, is dominated by the first emission. Let's consider for concreteness a quark

emitting a gluon, and work in the collinear regime (small R). In this approximation, we can consider the jet in isolation from the rest of the event, neglecting interference and splash-in, and we can approximate the QCD splitting functions with the singular portions. Doing so, the amplitude to radiate an extra parton can be written as

$$d\sigma_{n+1} \approx d\sigma_n \, dz \, \frac{dt}{t} \frac{\alpha_s}{2\pi} \mathcal{P}(z), \tag{2.9}$$

where t is the virtuality of the parent P, $z = E_q/E_P$ is the fraction of the parent energy retained by the daughter quark, and the splitting function $\mathcal{P}(z)$ for $q \to qg$ is given by

$$\mathcal{P}(z) = C_F \frac{1+z^2}{1-z}. \tag{2.10}$$

The parent virtuality t is of course the jet mass-squared. In the collinear limit,

$$t = E_P^2 z(1-z)\theta^2 = (p_{T,P} \cosh \eta)^2 z(1-z)\theta^2. \tag{2.11}$$

Integrating over rapidity, we can approximate the average jet mass-squared as:

$$\langle m^2 \rangle \approx p_{T,P}^2 \int_0^{R^2} \frac{d\theta^2}{\theta^2} \int dz \, z(1-z)\theta^2 \frac{\alpha_s}{2\pi} \mathcal{P}(z). \tag{2.12}$$

Note the limits on the θ integral: this is where the choice of jet algorithm enters. As established above, for all sequential jet algorithms, only radiation at angles smaller than R will be clustered into the jet. Strictly, we should use a running α_s evaluated at a scale set by the relative transverse momentum of the splitting, but to get a quick estimate, let's perform the integral in the approximation that α_s is constant. We then obtain

$$\langle m^2 \rangle \approx \frac{\alpha_s}{\pi} \frac{3}{8} C_F \, p_T^2 R^2. \tag{2.13}$$

The jet mass scales like p_T, as it had to, and is suppressed by $(\alpha_s/\pi)^{1/2}$. To this order the mass increases linearly with R. The exact value of the numerical coefficient will in general depend on the quark versus gluon content of the jet sample. For instance, the major QCD background for a doubly b-tagged boosted Higgs comes from the splittings $g \to b\bar{b}$, where the splitting function is

$$\mathcal{P}(z) = C_A(z^2 + (1-z)^2), \tag{2.14}$$

giving, in the constant-α_s approximation,

$$\langle m^2 \rangle \approx \frac{\alpha_s}{\pi} \frac{1}{20} C_A \, p_T^2 R^2. \tag{2.15}$$

Coming back to the Higgs, consider now a splitting $P \to ij$. We have $m^2 \approx 2p_i \cdot p_j \sim p_{T,i}p_{T,j}\Delta R_{ij}^2 = z(1-z)p_{T,P}^2\Delta R_{ij}^2$. In other words, just from kinematics we can express the opening angle in terms of the parent mass and p_T:

$$\Delta R_{ij} \sim \frac{m}{p_T}\frac{1}{\sqrt{z(1-z)}} \sim \frac{2m}{p_T}. \tag{2.16}$$

Now consider the k_T metric evaluated on this splitting $P \to ij$:

$$y_{ij} = \min(E_{T,i}^2, E_{T,j}^2)\Delta R_{ij}^2 = p_T^2 z^2 \Delta R_{ij}^2 \approx \frac{z}{1-z}m^2. \tag{2.17}$$

For jets with a fixed mass m, cutting on the splitting scale y_{ij} then can separate QCD jets, which have a soft singularity $\propto 1/z$, from boosted Higgses, which have a flat distribution in z. [1]

Moreover, a boosted Higgs will go from a mass m_H to massless daughters in one step, while QCD splittings prefer to shed virtuality gradually. To see this, consider the Sudakov form factor, which exponentiates the splitting functions to obtain the probability of evolving from an initial virtuality t_0 to a final virtuality t without branching:

$$\Delta(t) = \exp\left[-\int_{t_0}^t \frac{dt'}{t'}\,dz\frac{\alpha_s}{2\pi}\mathcal{P}(z)\right]. \tag{2.18}$$

Evaluating $\alpha_s = \alpha_s(t')$ and using an IR cut-off to regulate the splitting functions, at large t, one can work out that [11]

$$\Delta(t) \propto \left(\frac{t_0}{t}\right)^p \tag{2.19}$$

for an exponent $p > 0$, in other words, $\Delta(t) \to 0$ for large t. In other words, the probability of a QCD jet making a large jump in mass at a branching falls off as m^{-2p}. [2]

We have now identified two ways in which a Higgs boson H decaying perturbatively to $b\bar{b}$ will behave very differently from a QCD parton branching: the splitting will be symmetric, and show a sudden drop in parton mass. The search algorithm for finding a boosted Higgs looks for a splitting inside the Higgs jet that behaves like a perturbative decay, and works as follows:

---

[1]This is a little quick: not all QCD splitting functions have a soft singularity, and in particular $g \to q\bar{q}$ does not. However, $P_{g \to q\bar{q}}(z)$ is not flat in z, and in particular is minimized at the symmetric value $z = 1/2$, so cutting on y_{ij} can still help suppress this background.

[2]In fact, taking higher order corrections into account, one finds that the Sudakov form factor goes to zero even faster than polynomially for large t.

- Cluster the event on a large angular scale (Ref. [10] uses $R = 1.2$), using the C-A algorithm. Large angular scales are necessary in order to get good acceptance for collecting both Higgs decay products into a single fat jet: from Eq. 2.16, we can see that the b-$\bar{b}$ separation for a 125 GeV Higgs boson is $R_{b\bar{b}} \lesssim 1$ for $p_T \gtrsim 200$ GeV. We choose the C-A algorithm because it is a good compromise between accurately reflecting the shower structure of QCD, and minimizing sensitivity to soft radiation in the event.

- Now, given a hard fat jet, successively *unwind* the jet by undoing the cluster sequence one branching at a time. At each branching $P \to ij$, check to see whether the splitting looks sufficiently non-QCD-like, by asking that the branching be both *hard*,

$$\max(m_i, m_j) < \mu m_P \qquad (2.20)$$

  for some parameter μ, and *symmetric*,

$$y_{ij} > y_{cut} \qquad (2.21)$$

  for some choice of y_{cut}.

- If the splitting fails to be sufficiently hard and symmetric, discard the softer of i and j, and continue to unwind the harder.

- Continue until either an interesting splitting has been found or you run out of jet.

This procedure, often referred to as the "splitting" or "mass-drop" procedure, identifies an interesting Higgs-like splitting $H \to b\bar{b}$, which determines a characteristic angular scale $R_{b\bar{b}}$ for a particular event. Once this scale $R_{b\bar{b}}$ has been identified, we benefit greatly by using smaller scales to resolve the event, rather than the large $R = 1.2$ scale we started with.

The reason is the following: starting with such a large jet, we are guaranteed to sweep up a large amount of unassociated radiation along with the Higgs decay products. The effect of this unassociated radiation is to smear out the mass resolution. The invariant mass is especially vulnerable to distortion from even soft unassociated radiation, because evaluating $m^2 = E^2 - \vec{p}^2$ depends on large cancellations. The amount of distortion scales like

$$\frac{d\langle m^2 \rangle}{dR} \approx \Lambda_{soft} p_{T,J} R^3, \qquad (2.22)$$

in the approximation that unassociated radiation contributes a constant energy Λ_{soft} per unit rapidity: the jet area scales like R^2, while the incremental contribution to

the invariant mass from a soft particle at distance $R/2$ from the jet core contributes as $\Lambda p_{T,J} R/2$ [12]. So to recover mass resolution, it is vital to whittle down our initial fat jet to jets only as big as necessary to capture the radiation from the Higgs decay products.

In fact, we have already started whittling. The splitting procedure discards soft, wide-angle radiation clustered into the jet on its way towards finding the Higgs-like splitting. This by itself helps to clean up the mass resolution. But we can do better: given the scale $R_{b\bar{b}}$ which is our best guess at the angular separation of the Higgs' daughter particles, we can resolve the fat jet at the *filtering* scale $R_{filt} = \min(R_{b\bar{b}}/2, 0.3)$, and keep only the three hardest subjets. We keep three, rather than two, subjets in order to capture final-state radiation off of one of the b quarks.

Finally, demanding that the two hardest filtered subjets be b-tagged, Ref. [10] finds that the Higgs can be seen in this channel with 5σ significance in 30 fb^{-1} (at 14 TeV, combining $Z \to \ell^+\ell^-$, $Z \to \nu\bar{\nu}$, and $W \to \ell\nu$), and signal-to-background of $\mathcal{O}(1)$. However, we emphasize that *this and all other LHC phenomenological studies are based on expectations from Monte Carlo.* Even very sophisticated Monte Carlos necessarily capture only an approximation to the full physics of QCD. For this reason, both validation in data on one hand and formal theoretical study on the other are critical. Let us then end this section by showing a couple of the most important early experimental results. In Fig. 1, we show two plots from Ref. [13]. On the left, we see that shower Monte Carlos do a reasonable job of predicting the spectrum of jet masses for the QCD background. On the right, the jet mass is plotted as a function of the number of primary vertices N_{PV} in an event, or in other words, the amount of pileup. Note that after filtering, the jet mass has little to no dependence on N_{PV}, indicating that filtering is successfully isolating the hard process. Note also that filtering is *necessary*: prior to filtering, the dependence of jet mass on N_{PV} is significant, and in the 2012 operating environment average pileup multiplicity is $N_{PV} \gtrsim 30$.

Heartened by this evidence that our theoretical techniques have a reasonable relationship with reality, we will proceed in the next section to discuss more ideas for cleaning up pileup, and more jet properties which can discriminate signals from QCD backgrounds.
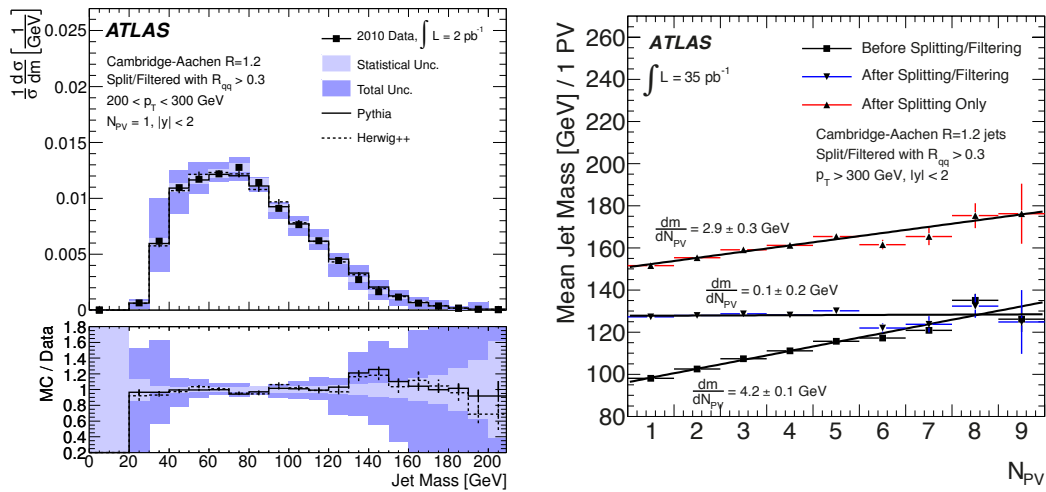
Figure 1: (Left) The distribution of jet mass for fat C-A jets (after splitting and filtering). Note the reasonable agreement between data and predictions from two different shower MCs. (Right) Average jet mass as a function of the number of primary vertices N_{PV}. Note that after filtering, the jet mass has little to no dependence on N_{PV}. From Ref. [13].

3   Lecture II: Jet Grooming and Jet Shapes

Our last section concluded with a walk-through of the pioneering boosted Higgs study, where we saw examples of two topics we will be discussing in this lecture, namely jet grooming and jet shapes.

3.1   Jet grooming

In the boosted Higgs analysis discussed in the previous lecture, we saw that jet mass resolution was badly degraded by the presence of unassociated radiation in the jet, and introduced the process of *filtering* to mitigate these contributions. Filtering is one of several *jet grooming* algorithms, all of which are designed to "clean up" jets by subtracting the contributions of unassociated radiation.

Trimming   [14], similarly to filtering, reclusters the constituents of a fat jet and retains a subset of the subjets, but has a different criterion for keeping subjets. For each jet of interest, the algorithm is:

- Recluster the constituents using some jet algorithm (the original reference specifies k_T), and resolve on a fixed small angular scale R_0.

14

- Keep each subjet i that passes a p_T threshhold,

$$p_{T,i} > f\Lambda_{hard} \qquad (3.23)$$

  for a cutoff parameter f_{cut} and a hard momentum scale Λ.

- The final trimmed jet is the sum of the retained subjets.

The essential idea is that radiation we want to keep tends to be distributed in clusters, reflecting a parent parton emission, while unassociated radiation we don't want to keep is more uniformly distributed. Asking that radiation cluster sufficiently on small scales then preferentially picks out the radiation which ultimately originated from a parent hard parton. The k_T algorithm was originally proposed here because it increases the chances that soft FSR will be kept: since clustering in the k_T metric works from soft up, using k_T increases the chance that a relatively soft parton emitted in the parton shower will be reconstructed and pass above the p_T threshold. But it is possible to imagine using other algorithms for the small-scale reclustering, and indeed implementations using C-A [15] or even anti-k_T [16] have been seen to be effective.

The trimming algorithm is simple to state; the detailed questions arise when we ask how the parameters should be chosen, and in any particular application parameter choices should be optimized for the specific process under consideration. Typical values for the small angular scale range between $0.2 \leq R_0 \leq 0.35$; for R_0 much smaller than $R_{min} = 0.2$, the finite angular resolution of the calorimeter starts to introduce irregularities. Good choices for Λ are either the total jet p_T, for dijet events or other such events where all jets have similar p_Ts, or the scalar sum transverse energy of the event, H_T, if jets have some spread over a broader range of p_Ts. Typical values for the cutoff parameter f_{cut} range between 10^{-2} (more typically for jet p_T) and 10^{-3} (for event H_T): this tends to work out to keeping subjets down to a 5 to 10 GeV threshold.

Pruning [17, 18] builds on the observation that the mass-drop algorithm improves mass resolution on boosted hard decays even before the filtering step, by discarding soft wide-angle radiation clustered into the fat jet at the final stages. In the C-A algorithm, the typical last clusterings in the fat jet are of stray soft radiation, usually unassociated with the parent particle, at wide angles to the jet core. These late, wide-angle clusterings have a disproportionate effect on jet mass.

Pruning adapts the splitting algorithm to specifically check for soft, wide-angle splittings, and throw them away. The algorithm is:

- Given a jet J, recluster its constituents with C-A, and then sequentially unwind the cluster sequence.

- At each splitting $P \to ij$, check whether the splitting is both *soft*,

$$z = \frac{\min(p_{T,i}, p_{T,j})}{p_{T,P}} < z_{cut},$$ (3.24)

  and at *wide angle*,

$$\Delta R_{ij} > D_{cut}.$$ (3.25)

  If so, then drop the softer of i, j, and continue unwinding the harder.

- Stop when you find a sufficiently hard (or collinear) splitting.

Again, this algorithm has parameters that must be optimized specifically for each process under consideration. Typical values of z_{cut} are $z_{cut} \approx 0.1$, while the radial separation should be tuned to the expected opening angle for a hard process, $D_{cut} \approx 2m/p_T \times 1/2$.

Grooming in action. All three grooming techniques (filtering, trimming, and pruning) improve signal to background by both improving mass resolution for signal *and* suppressing QCD background. QCD jets, whose jet masses are generated by relatively softer and less symmetric emissions, are more likely to have their masses shifted substantially downward by jet grooming than collimated perturbatively decaying particles are, thus depleting the background to high-mass searches. Both the sharp gain in signal mass resolution and the depletion of the high mass background can be seen in Fig. 2.

We can also see in Fig. 2 that the different grooming techniques all act slightly differently on background massive QCD jets[15]. QCD jets with high masses dominantly have this mass generated by a relatively hard perturbative emission, which all algorithms are designed to retain, so performance between the different algorithms is similar. However, the effects of the different grooming algorithms on QCD backgrounds are still sufficiently distinct that some benefit can be obtained in applying multiple grooming algorithms [19].

At low masses, the differences between the grooming algorithms become more pronounced. QCD jets at low masses are dominated by a hard core. Filtering keeps a fixed number $N = 3$ of subjets, and therefore retains relatively soft radiation. Trimming, by contrast, will typically drop all radiation except that within R_{sub} of the jet core. Pruning will also typically drop all but the radiation in the core, but the resolution radius D is set to scale like m/p_T, and therefore $D \to 0$ as $m \to 0$. Thus at small masses typically $R_{prune} < R_{sub}$, so pruning acts more aggressively than trimming.
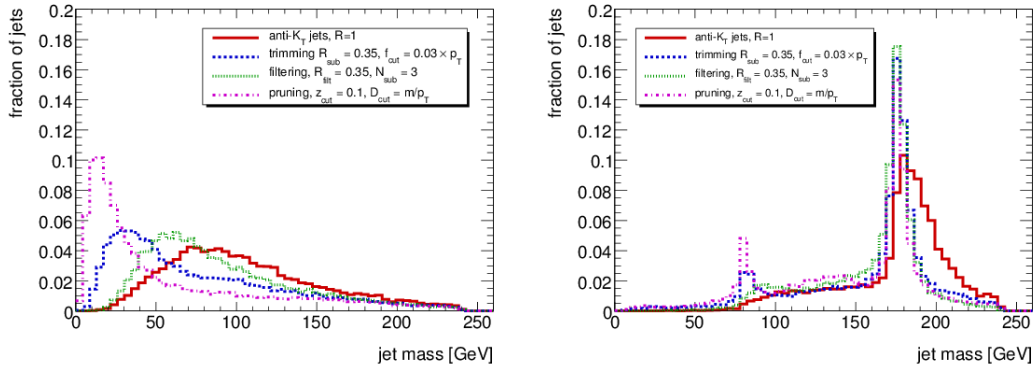
Figure 2: The operation of filtering (green, dotted), trimming (blue, dashed), and pruning (purple, dash-dotted) on background QCD jets (left) and boosted top jets (right). From Ref. [15].

3.2 Jet Shapes

Another feature of the boosted Higgs analysis we saw in the previous lecture was the importance of *jet mass*, which allowed us to concentrate signal in a sharp peak on top of a falling background [20]. Jet mass is an example of a *jet shape*: a function f defined on a jet J that quantifies the properties of the jet without the (explicit) use of any jet algorithm. The approach is conceptually akin to *event shapes*, which allow quantitative study of QCD without requiring specific characterization of an event in terms of jets, and indeed many jet shapes are descendants of event shapes.

Before discussing individual jet shapes, let us make two general comments. First, as we saw for jet mass, jet shapes are vulnerable to the inclusion of unassociated radiation, particularly pile-up, into jets, to a greater or lesser extent depending on the particular jet shape, and the sensitivity of the jet shape to unassociated radiation can be important. Second, one should bear in mind that any reasonable jet shape needs to be both infrared- and collinear-safe. Any linear function of particles' p_T is automatically safe; factorization theorems for other jet shapes can be proven [21].

3.2.1 Radial distribution of particles within a jet

The probability of a showering parton to emit a daughter parton depends on the running coupling α_s evaluated at the $k_\perp$ scale of the splitting. Jet shapes which measure the angular distribution of particles in an event are therefore measuring both the strength and the running of the strong coupling constant, and are classic probes of QCD. These

jet shapes are also sensitive to the color charge of the parent parton: since $C_F < C_A$, an initial gluon will radiate more, and at wider angles, than an initial quark.

Jet Broadening is a classic e^+e^- observable. Given a thrust axis $\hat{n}$, we can partition the particles i in an event into hemispheres according to $\text{sign}(\vec{p}_i \cdot \hat{n})$, which for dijet-like events is equivalent to associating each particle to a jet. Hemisphere broadening is then defined as the momentum-weighted transverse spread of the particles,

$$B_H = \frac{1}{\sum_{i \in H} |\vec{p}_i|} \sum_{i \in H} |\vec{p}_i \times \hat{n}| \tag{3.26}$$

where the sum runs over all particles i in a hemisphere H.

Differential and Integrated Jet Shapes are, thanks to a historic quirk of nomenclature, names for two specific jet shapes: the so-called *differential jet shape* $\rho(r)$ and the *integrated jet shape* $\Psi(r)$, which characterize the radial distribution of radiation inside a jet. These jet shapes are also sometimes called the *jet profile*. Both of these shapes are defined on an ensemble of N jets formed with radius R. Then for $r < R$, the integrated jet shape $\Psi(r)$ is the ensemble average of the fraction of a jet's p_T which is contained within a radius r from the jet axis. Defining r_i as the distance of a constituent i from the jet axis,

$$\Psi(r) = \frac{1}{N} \sum_J \sum_{i \in J} \frac{p_T(0 < r_i < r)}{p_{T,J}}. \tag{3.27}$$

Here the second sum runs over all constituents i of a jet J. The differential jet shape $\rho(r)$ is then given by

$$\rho(r) = \frac{1}{\delta r} \frac{1}{N} \sum_J \sum_{i \in J} \frac{p_T(r < r_i < r + \delta r)}{p_{T,J}}. \tag{3.28}$$

These variables are often included in the suite of QCD precision measurements performed by experimental collaborations, as for instance in the ATLAS study [22], and are useful for validating parton shower models.

Girth is another jet shape which probes the radial distribution of radiation inside a jet. Let r_i again be the distance between a constituent i and the jet axis. Then the girth of a jet g_J is the linear radial moment of the jet,

$$g_J = \sum_{i \in J} \frac{p_{T,i} r_i}{p_{T,J}}. \tag{3.29}$$

In the collinear limit $\theta \to 0$, girth becomes equivalent to jet broadening (where the thrust axis is replaced by the jet axis). Girth has been shown to be particularly useful for distinguishing quark-initiated jets from gluon-initiated jets [23].

Angularities [24] are a related family of jet shapes, defined as a function of the parameter a:

$$\tau_a = \frac{1}{2E_J} \sum_{i \in J} p_{\perp,i} e^{(a-1)\eta_i}. \tag{3.30}$$

Here η_i is the separation in rapidity only between particle i and the jet axis, and $p_{\perp,i}$ the momentum transverse to the jet axis.

3.2.2   Discriminating boosted decay kinematics

The radial distribution jet shapes discussed in the previous section are geared toward probing the characteristic shower structure of QCD. Here we will discuss several examples of jet shapes which target evidence of non-QCD-like substructure in jets.

Planar flow [24] considers the spread of the jet's radiation in the plane transverse to the jet axis (see also the closely related *jet transverse sphericity* shape [25]). Since QCD showers are angular-ordered, radiation subsequent to the first emission $P \to ij$ tends to be concentrated between the clusters of energy defined by i and j, leading to a roughly linear distribution of energy in the jet. By contrast, boosted three-body decays, such as boosted tops, have a more planar distribution of energy.

Define the tensor

$$I^{ab} = \frac{1}{m_J} \sum_{i \in J} \frac{p_{i,\perp}^a p_{i,\perp}^b}{E_i}, \tag{3.31}$$

where the indices a, b span the plane perpendicular to the jet axis, and $\vec{p}_{i,\perp}$ denotes the projection of particle i's momentum into this plane. Letting λ_1, λ_2 be the eigenvalues of I^{ab}, the planar flow of a jet is given by

$$Pf_J = \frac{4\lambda_1 \lambda_2}{(\lambda_1 + \lambda_2)^2} = \frac{\det I}{(\text{Tr} I)^2}. \tag{3.32}$$

With this normalization, $Pf_J \in (0,1)$. Monte Carlo studies have demonstrated that QCD events do indeed peak at low values of Pf, while boosted top decays show a relatively flat distribution in Pf, but preliminary results show some sensitivity to shower modeling [25] and the utility of this shape in data is so far unclear.

19

Note that neither I^{ab} nor its eigenvalues are invariant under longitudinal boosts. For fully reconstructible events this is not a worry in theory, as all events can be considered in the reconstructed CM frame, but finite experimental resolution can become an issue in transforming from the lab frame into the CM frame.

Template overlaps define jet shapes based on (aspects of) the matrix elements for boosted object decays [26]. For example, consider the three body top quark decay with intermediate on-shell W. The phase space for this decay is (in the narrow-width approximation) determined by four parameters, which can be parameterized as the solid angle governing the two-body decays of both the t and its daughter W. Note that (1) the azimuthal angle ϕ_t is meaningful, as the detector geometry is not invariant under rotations around the top direction of motion, and (2) this phase space has both m_t and m_W built in. A series of templates describing this phase space can be generated by discretizing the four-dimensional space. To use these templates on a jet, the method of template overlaps finds the template which has best overlap with the kinematic configuration of the jet constituents according to a chosen metric. The ultimate variable is the numerical value of the best overlap, which distinguishes between QCD jets and boosted tops.

N-subjettiness [27] takes a different and more general approach to probing jet substructure via jet shapes. Given N axes $\hat{n}_k$, we define N-subjettiness as

$$\tau_N = \frac{\sum_{i \in J} p_{T,i} \min(\Delta R_{ik})}{\sum_{i \in J} p_{T,i} R_0} \tag{3.33}$$

where R_0 is the jet radius, and ΔR_{ik} is the distance between particle i and axis $\hat{n}_k$. The smaller τ_N is, the more radiation is clustered around the chosen axes, or in other words, smaller values of τ_N indicate a better characterization of the jet J as having N (or fewer) subjets. Conversely, if τ_N is large, then a description in terms of $> N$ subjets is better.

However, as QCD alone will happily make jets with subjets, to differentiate boosted objects we need to probe not just the possible existence of subjets, but their structure. The real distinguishing power of N-subjettiness occurs when looking at *ratios*. For instance, a two-prong boosted particle such as a Higgs or W will have large τ_1 and small τ_2. QCD jets which have small τ_2 will generically have smaller τ_1 than for signal, as the QCD jets are more hierarchical; conversely, QCD jets which have large τ_1 are generally diffuse, and will have larger τ_2 as well than for signal. Thus the best single

discriminating variable is τ_2/τ_1, or, more generally

$$r_N = \frac{\tau_N}{\tau_{N-1}} \tag{3.34}$$

for a boosted N-prong particle.

The question of how to determine the input subjet axes $\hat{n}_k$ is an interesting one. One approach, which is fast and perfectly serviceable for most applications, is to use a jet algorithm, such as exclusive k_T, to determine subjet axes. Naturally, the results then retain some dependence on the choice of jet algorithm used to find the axes. Another approach is to marginalize over all possible choices of $\hat{n}_k$, and choose the set which minimizes τ_N [28]. While this choice is computationally more intensive, it removes the dependence on the jet algorithm choice, and additionally guarantees the nice property that

$$\tau_{N-1} > \tau_N, \tag{3.35}$$

which holds only approximately if fixed subjet axes are used.

N-subjettiness is a conceptual descendent of the event shape N-jettiness [29], which classifies events as being N-jet-like without reference to jet algorithms.

3.2.3   Color flow variables

Beyond kinematics, boosted perturbative decays can also differ from QCD backgrounds in their color structure. Consider a color singlet such as a H or W boson decaying to a quark-antiquark pair. The daugher quark jets form a color dipole: they are color-connected to each other, but not to the rest of the event. Meanwhile, the backgrounds to these processes come from QCD dijets, which necessarily have different color connections, as we show in Fig. 3, where the radiation patterns for a color-singlet signal are plotted on the left and for a typical background on the right, as computed in the eikonal (soft) approximation. This observation has motivated work on variables which can add color flow to the suite of features which can discriminate signal from background.

Jet pull [30] defines for each jet a transverse vector $\vec{t}_J$ characterizing the net directional distribution of the soft radiation surrounding the jet core. Defining $\vec{r}_i$ as the (transverse) direction of particle i from the jet axis, the pull vector is

$$\vec{t}_J = \sum_{i \in J} \frac{p_{T,i}|r_i|\vec{r}_i}{p_{T,J}}. \tag{3.36}$$

The direction of $\vec{t}_J$ relative to other jets in the event then is sensitive to the color connection of the jet J. Two jets which are color-connected to each other will have pull
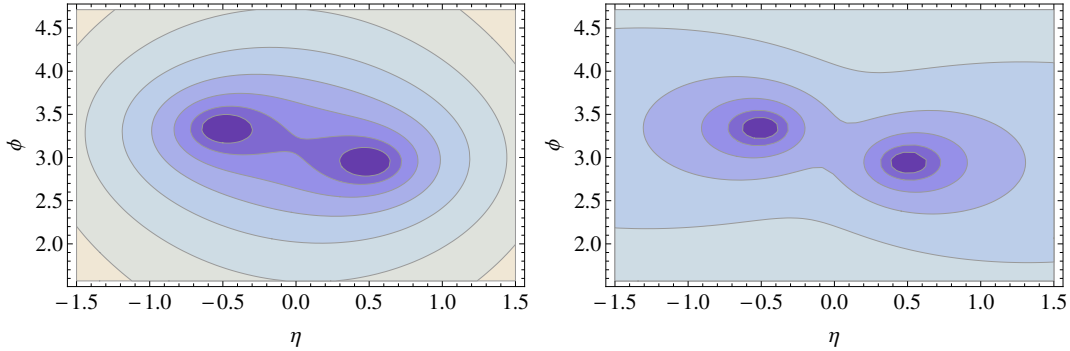
Figure 3: Radiation patterns in the eikonal approximation for two triplet color sources color-connected to each other (left) and to the beam (right). Contours are logarithmic, and the scales in the two figures are not the same.

vectors pointing toward each other. Jets which are color-connected to the beam will have pull vectors pointing toward the beam. Once two interesting (sub)jets have been identified, the discriminating variable is then $\cos\theta_t$, the angle between the pull vector and the line connecting the two (sub)jet cores. An initial experimental study of pull has been carried out at D0, using the W in top events [31].

Dipolarity [32] is a jet shape which is designed to test for color dipole-like structure when the apparent particle is boosted and the two (sub)jets of interest are geometrically nearby. Since pull scales like r_i^2, it can be unduly sensitive to the detailed assignment of particles between the two (sub)jet cores to one or the other of the two (sub)jets. Dipolarity therefore uses as the relevant distance measure R_i, the transverse distance of particle i to the line segment connecting the (sub)jet cores,

$$D_J = \frac{1}{p_{T,J}R_{12}^2} \sum_{i\in J} p_{T,i} R_i^2.$$

(3.37)

Note that dipolarity requires input (sub)jet axes. The major application studied to date has been in boosted top tagging, where dipolarity can improve the identification of the boosted daughter W.

Keeping the right soft radiation. We have emphasized the need for jet grooming tools in the busy, high luminosity environment of the LHC. However, that grooming will groom away most if not all of the information about color flow. To use the information contained in an event's color flow, it is necessary to retain at least some of the soft

radiation. Exactly which soft radiation is included, and at which stage in the analysis, is a question which has to be addressed case-by-case. As an example, we will discuss how the dipolarity shape can be incorporated into a boosted top tagger [32]. Top tagging will be discussed at length in the next section; for the moment, it suffices to think of a top tagger as an algorithmic black box which acts on a fat jet to return candidate b, j_1, and j_2 subjets, and discards some radiation in the process.

The returned subjet axes define the characteristic opening scale, R_{12}, and provide the input axes for the dipolarity jet shape. As the top-tagger has discarded some of the radiation associated with the top quark in identifying the candidate subjets, to evaluate dipolarity we will need to go back to the original fat jet and include a larger subset of particles. Clearly, the radiation we'd like to include when evaluating the dipolarity of the candidate W daughters is only that associated with the two light quark jets; including radiation originating from the b would just skew the results. Let us consider only moderately boosted tops, such that the b jet is not overlapping with the other two. From the angular-ordered property of QCD showers, we know that in top events, all radiation associated with either light quark must be at angular separations less than the opening angle of the dipole, $\Delta R < R_{12}$. Thus, all radiation from the W is contained in cones of radius R_{12} around each light quark jet. The authors of Ref. [32] find that keeping all radiation within these two cones is casting too wide a net, however, and a smaller cone size of $R_{12}/\sqrt{2}$ is a better tradeoff between keeping all the radiation from the W and avoiding pollution from pileup, underlying event, and splash-in from the nearby b.

Color flow variables capture a genuine physical difference between signal and background. They have been shown, in theoretical work, to make a sizeable impact in signal significance [16, 45, 32, 33], and show great promise as tools to expand our understanding of SM and BSM physics. It is important to bear in mind, however, that these "proof of principle" analyses have all been performed using shower Monte Carlos, which capture only leading approximations to the full QCD dynamics. Just as the jet shapes discussed in section 3.2.1 above have been and are still important tools for assessing the validity of the approximations made in the Monte Carlo generators, measuring and calibrating color flow variables in data is critical to understand the validity of the shower models and the performance of any color flow variable. This experimental program is, as of yet, in its infancy. In the meantime, theoretical studies should bear this uncertainty in mind. To estimate the uncertainties, it is useful (as it is for any novel substructure variable) to check results using more than one shower model.

4 Lecture III: Top tagging and searches for physics BSM

In this section we will assemble the tools and techniques developed in the previous two sections and apply them to searches for physics beyond the standard model. By far the most universally motivated application of jet substructure techniques to BSM physics is in the hunt for TeV-scale new states which decay to electroweak-scale SM particles. The best reason for new physics to live anywhere near the weak scale is that it is partially responsible for the generation of the electroweak scale. New physics that is related to EWSB will naturally couple most strongly to those particles in the SM which feel EWSB most strongly, in particular the top quark and the EW bosons (H, W, and Z), and thus will decay preferentially to these heavy particles rather than to the light quarks and leptons which yield simpler final states. Moreover, we have compelling reasons to believe new physics will naturally decay to *boosted* SM particles. Even before the LHC turned on, the lack of deviations from SM predictions for flavor or precision electroweak observables already hinted that the likely scale for new physics was not v_{EW} as naturalness might have suggested, but rather $\Lambda \gtrsim$ few TeV. Evidence for this "little hierarchy" problem has of course only gotten stronger as the LHC has directly explored physics at TeV scales. Thus many models which address the stabilization of the EW scale will naturally give rise to final states rich in boosted tops, Higgses, W's and Z's.

In this section we will provide an introduction to top tagging at the LHC, followed by a few brief concluding comments on searching for more general BSM physics with jets.

4.1 Top Tagging

As we established in Section 1, top pair production at the LHC covers a broad range of kinematic regimes interpolating between threshold ($\sqrt{s} = 2m_t$), where tops are well described as a six-object final state, up to TeV-scale energies, where the tops are highly collimated and are best described as a two-object final state. Top reconstruction must thus be able to flexibly cover a wide range of kinematic scenarios. In the interest of time, we will restrict our attention here to top taggers which target the hadronic decay of the top quark, although the semi-leptonic decay mode also requires interesting techniques for identification and reconstruction [34, 35].

As for jet algorithms, the "best" top tagger depends on the question being asked. In particular, different strategies are required at high p_T ($\gg m_t$) versus moderate p_T ($\gtrsim$

m_t). Another question is: what signal efficiency is necessary? Every tagging technique trades off signal efficiency against background mistag rate. Depending on the search in question, the composition of the backgrounds will change, and therefore the necessary mistag rate will shift as well. For example, consider a top pair event with at least one boosted hadronic top. If the other top is also hadronic, then QCD dijets are by far the dominant background, and small QCD mistag rates are required. But if the other top is leptonic, then $W+$ jets becomes an important background, and if the top is produced in association with some new physics objects, such as $\not{E}_T$, then the backgrounds may be substantially smaller, and mistag rates may be entirely unimportant.

The aim of this section is to provide an introduction to top tagging by discussing a representative variety of top taggers. Specifically, we will consider the top taggers currently used by both LHC experiments, which work best in the highly boosted regime; the "HEP top tagger", which targets moderate p_T; and top tagging with N-subjettiness.

4.1.1 CMS top tagger

The hadronic top tagger used by CMS [36] is largely based on the "Hopkins" top tagger [37]. It builds on the techniques of the boosted Higgs "splitting/filtering" or "mass drop" analysis, which we discussed in Section 1. Thus, we again begin by clustering the event using the C-A algorithm, on large angular scales, capturing all of the top decay products in a single fat jet, which we will then unwind until we find interesting substructure. Compared to the Higgs analysis, there are two important differences. First, we are looking for at least three hard subjets, instead of two. Second, we take the fat jet radius to be noticeably smaller than we did for the Higgs case: $R = 0.8$. Using our rule of thumb, $R \sim 2p_T/m$, this means we are targeting tops with $p_T \gtrsim 500$ GeV: appropriate for production from a TeV-scale resonance. Contrast this with the boosted Higgs, which was targeting the high-p_T tails of SM associated production, where requiring large p_T imposed a significant price in signal acceptance.

Iteratively declustering the fat jet, we encounter splittings $P \to ij$. Our criterion for an interesting splitting is simply that both daughter subjets must carry a sufficiently large fraction of the *total* fat jet momentum,

$$p_{T,j} > \delta_P \, p_{T,J} \tag{4.38}$$

for some parameter δ_P. If a splitting fails to meet this criterion, discard the softer of i, j, and continue to unwind the harder. The splitting is rejected if it is too collinear, $|\Delta\eta_{ij}| + |\Delta\phi_{ij}| > \delta_R$, for another parameter δ_R. This procedure stops when either both i, j are softer than $\delta_P \, p_{T,J}$, or only one particle is left.
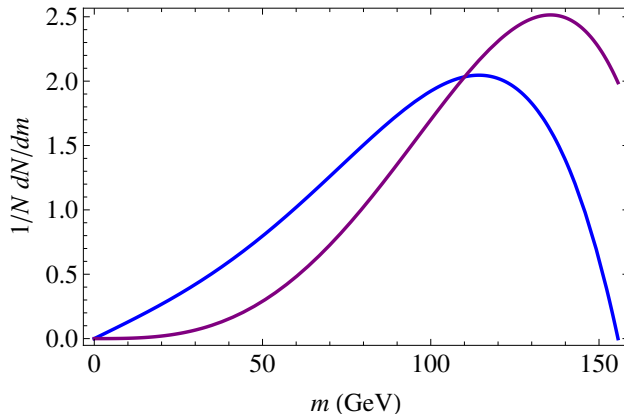
Figure 4: Leading order distributions of $m_{b\bar{d}}$ (blue) and m_{bu} (purple) in unpolarized top decay.

If an interesting hard, non-collinear splitting $P \to j_1 j_2$ is found, then the next step is to successively unwind both j_1 and j_2 according to the same algorithm, in search of further interesting splittings. This procedure returns a set of 2, 3, or 4 subjets. Fat jets returning only 2 subjets don't have enough substructure to be good top candidates, and are rejected. Jets which return 3 or 4 subjets do show enough substructure to be interesting, and the next step is to test whether or not they also have top-like kinematics.

As for the Higgs, the single most important discriminator is the jet mass. CMS requires that the jet mass, as computed from the sum of the returned subjets, lie within a top mass window, $m_t - 75\,\text{GeV} < m_J < m_t + 75$ GeV.

The onshell decay of the W inside the jet will also help us separate signal from background, but rather than trying to explicitly identify a pair of subjets which reconstruct a W—a procedure highly vulnerable to the misassignment of particles in overlapping jets—we will exploit the presence of the W mass scale in a less direct way.

The pairwise invariant masses of all possible combinations of the three daughter quarks are all governed by the mass scales in the top matrix element, m_W and m_t. The distribution of the invariant mass of the b and the $\bar{d}$-type quark (equivalent to the charged lepton in leptonic top decay) is shown in Fig. 4. The most likely value of $m_{b\bar{d}}$ is approximately 115 GeV. The invariant mass of the b and the u-type quark (equivalent to the neutrino) is peaked at even larger values. By contrast, subjet masses from QCD background processes are hierarchically smaller than the total parent jet mass. Thus instead of trying to reconstruct the W, we simply require that the *minimum* of the invariant masses formed from pairs of the three hardest subjets be sufficiently large to

reject backgrounds,

$$\min(m_{12}, m_{13}, m_{23}) > 50 \,\text{GeV}. \tag{4.39}$$

These cuts on masses, together with the substructure requirement, constitute the tagger. Note that no b-tagging information is used. Tagging b-jets is very difficult in this environment for two reasons. First, the b is embedded in a highly collimated top, so disentangling the tracks that are associated with the b from the other tracks in the jet is challenging. Second, the b itself is at very high p_T, so the opening angles of its daughter products are small, and it is difficult to get sufficient resolution from the reconstructed tracks to reconstruct the displaced vertex. Note also that the tagger doesn't require jet grooming. This is partly because the iterative decomposition procedure is performing some of that function in its own right, as it discards soft wide-angle radiation in the process of finding hard subjets (compare pruning). The smaller geometric size of the fat jets also means that pollution is not as large an effect.

4.1.2 ATLAS top tagger

We turn next to the ATLAS top tagger. Like CMS' tagger, it is optimized for high p_T, and like CMS' tagger, it is based on iterative declustering of a sequential algorithm. However, the ATLAS tagger draws on a very different set of ideas, largely based on work by Ref. [38] and the "Y-splitter" of Ref. [39].

The ATLAS top tagger begins by clustering events using the anti-k_T algorithm with $R = 1.0$. (The slightly larger jet radius means that this tagger works best at slightly lower p_T than does the CMS tagger.) Since the anti-k_T algorithm knows nothing about the singularity structure of QCD, its use is simply to identify a nicely regular initial set of particles. The next step is to take this set of particles and recluster them using the k_T algorithm.

Recall that the k_T algorithm preferentially clusters soft splittings. This means that the hardest splittings in the jet are the very last ones. Thus, there is no need to do any preliminary unwinding, and the existence of hard substructure is directly reflected in the hardness of the scales given by the k_T metric evaluated on the last few splittings in the jet:

$$d_{ij} = \min(p_{T,i}^2, p_{T,j}^2)\Delta R_{ij}^2. \tag{4.40}$$

Large splitting scales mean the emissions are both hard and at wide angles. The ATLAS tagger uses as inputs the splitting scales of the last three recombinations, d_{12}, d_{23}, and d_{34}. The first two splittings correspond (usually) to the identification of the three daughter partons, and the third to possible FSR from one of the partons. Since for tops

the splitting d_{34} is the first which comes from the QCD shower, its scale can still be relatively large; on the other hand, for background QCD jets, the hierarchical nature of the shower means that generally $d_{34} \ll d_{23} \ll d_{12}$. Thus cuts on d_{34} maintain some discriminating power.

However, instead of cutting directly on the massive splittings d_{ij}, it is advantageous to change variables to a set which are less correlated with the jet and subjet invariant masses [25]. We define the energy sharing variables

$$z_{ij} = \frac{d_{ij}}{d_{ij} + m_{ij}^2} \approx \frac{E_j}{E_i + E_j} \tag{4.41}$$

where in the last step we have taken the collinear limit (and $p_{T,i} > p_{T,j}$). Notice that by performing this change of variables we have removed sensitivity to the collinear singularity, so that z_{ij} is only capturing information about the soft singularity. Meanwhile, jet invariant masses still retain information about the relative angles between the jets, so the correlation between the variables has been reduced.

The final set of variables that make up the ATLAS top tagger is then:

- The total jet mass, m_J. The tagger requires $m_J > 140$ GeV, and no upper bound: no grooming procedure is used, so the mass spectrum is distorted upwards.

- The variable Q_W, defined as the minimum pair invariant mass of the three subjets identified at the splitting scale d_{23}. This is the equivalent to cutting on the minimum pair invariant mass in the CMS tagger; only the method of finding the subjets is different. We require $Q_W > 50$ GeV.

- All three energy sharing variables, z_{12}, z_{13}, and z_{23}, which are subject to numerical cuts.

4.1.3 HEP top tagger

We turn now to the Heidelberg-Eugene-Paris top tagger, which functions on tops with $p_T \gtrsim 200$ GeV [40, 41]. In some sense this algorithm is more of an event reconstruction strategy than a top tagger. The algorithm begins by clustering the event using C-A on the extremely large angular scale $R = 1.5$, and requiring the fat jets thus formed to have $p_T > 200$ GeV. The p_T cut of 200 GeV puts us in the regime where the top is sufficiently boosted that its decay products will frequently lie in a single hemisphere. Looking at extremely fat jets is effectively identifying hemispheres in an event while avoiding the need to set any fixed angular scales for resolution within those hemispheres. This is

an effective strategy for tops in this intermediate kinematic regime, where events will straddle any fixed angular scale; by unwinding C-A hemispheres, we allow the angular scales to be flexibly identified event by event.

The next step is to unwind the fat jet looking for interesting hard structure. This is done by employing a (loose) mass-drop criterion. For a splitting $P \to ij$, with $m_j < m_i$, the splitting is deemed sufficiently interesting if

$$m_j > 0.2\, m_P. \tag{4.42}$$

If the splitting passes this criterion, retain both i and j in the list of jets to unwind; otherwise, discard j and keep unwinding i until $m_i < 30$ GeV, at which point the unwinding stops. This unwinding procedure is performed on all subjets identified as interesting via Eq. 4.42. The output of this step is a list of subjets $\{j_i\}$ resulting from this iterative declustering; if there are at least 3 such subjets, then we have found enough substructure to continue.

At the next stage, we *filter* the substructures to shrink the geometric area associated with the top daughters and thereby reduce sensitivity to pileup, etc. Unlike in the Higgs case, where the mass drop criterion identified a unique angular scale $R_{b\bar{b}}$ associated with the sole hard splitting, we have a more complicated set of jets with more than one interesting splitting, and it is not immediately obvious which angular scale should be used to filter the event. The HEP top tagger determines the filter radius R_{filt} by brute force, as follows. For each possible set of three subjets that can be drawn from the $\{j_i\}$, filter them by resolving the constituents of those subjets with radius $R_{filt} = \min(0.3, \Delta R_{ij})$, and retain up to five subjets. Let m_{filt} be the invariant mass of these up-to-five filtered subjets, and select the set with m_J closest to m_t as the top candidate. These up-to-five filtered subjets are then (yet again) reclustered into three subjets, which are the candidates for the partonic top daughters.

The next step is to test whether or not the reconstructed top daughters have top-like kinematics. Again, we will exploit the presence of both the top and W mass scales. We have already used m_t to identify the best set of subjets. Unlike in the previous taggers, we will now demand evidence of the on-shell W in a more complex way. Label the three subjets returned by the previous step as $\{j_1, j_2, j_3\}$ in descending order of p_T. Of the three invariant masses m_{12}, m_{13}, and m_{23}, only two are independent. This means that the top kinematics is characterized by a specific distribution in the two-dimensional space determined by the pair invariant masses. Top jets are focused into a thin triangular annulus in this space, as two subjets reconstruct an on-shell W (the annulus is triangular since any of the m_{ij} may correspond to the W). Background, by
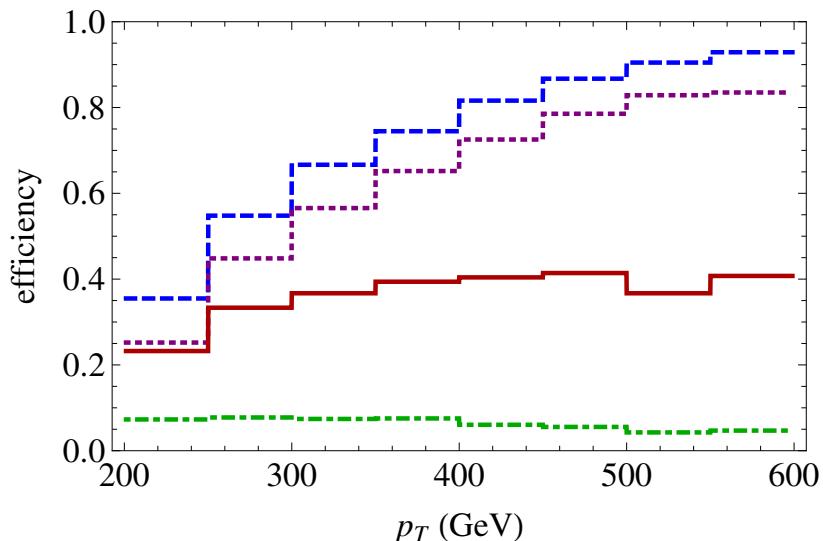
Figure 5: HEP top tagger efficiencies on top quarks for: all top decay products within $\Delta R = 1.5$ of each other (blue, dashed); all top decay products clustered into $R = 1.5$ C-A fat jets (purple, dotted); tagged by the HEP top tagger (red, solid); tagged, but with reconstructed subjets not matching original partons (green, dot-dashed). Data from Ref. [41].

contrast, is concentrated in regions of small pairwise invariant masses. The kinematic cuts imposed in the HEP top tagger pick out this top-like triangular annulus by asking that events lie on one of the three branches of the annulus.

To understand how well this procedure covers the interpolating kinematic region, we plot efficiencies for tops to pass through these steps in Fig. 5. As is evident from the blue (dashed) curve, simply demanding that all decay products of the top lie in a single hemisphere imposes a non-negligible acceptance price for tops at the low end of the p_T range, which drops quickly as the tops become more energetic. Further demanding that the top daughters all be clustered into the same fat jet results in an additional mild efficiency loss, seen in the purple (dotted) curve. The purple curve is the fraction of tops giving rise to taggable jets (neglecting the possibility of mistagged signal). The red line denotes the final efficiency of the full HEP top tagger, after the filtering and kinematic cuts. At low p_T, the fraction of taggable jets which are in fact tagged is near unity, but as the tops become more collimated, the probability of a taggable jet passing the kinematic cuts falls off, in large part because collimation and jet-particle misassignment make the W mass reconstruction less precise. At the upper end of the p_T range shown in

the figure, the high-p_T top taggers are useful, and would take over. Let us also comment that there is a possibility for tops to pass the top tagger by accident, when the algorithm picks up the wrong set of jets; this is shown in the green (dot-dashed) curve.

4.1.4 N-subjettiness

As we saw in section 3.2.2, N-subjettiness offers an entirely complementary test of the existence of hard substructure. A simple and highly effective top tagger can be constructed using as input variables just the jet mass and the ratio τ_3/τ_2. Further refinement is possible with a multivariate analysis which uses in addition τ_2/τ_1 as well as τ_1, τ_2, and τ_3 individually [28].

From our experience with the previous taggers, we can guess that even further improvement would be possible if some information about the W were also incorporated; since the N-subjettiness jet shape also provides a method of determining subjet axes, it naturally suggests methods for defining three subjets and computing the analog of Q_W. To the best of the author's knowledge, no such study has been publicly performed.

4.1.5 Top tagging performance

Let us now consider the performance of the top taggers which we have discussed. This task is made easier by the work performed in the BOOST 2010 [15] and BOOST 2011 [42] workshops, which compared the performance of different top taggers on the same reference sets of event samples. These event samples are publicly available online, so should you develop your own brilliant ideas about top tagging, you can cross-check the performance of your novel technique with the techniques already in the literature. In Fig. 6 we show performance curves for the high-p_T top taggers which we discussed above. Overall, these high-p_T top taggers have efficiencies on the order of $\epsilon \sim 50\%$, at a (QCD) background mistag rate of $\epsilon_{fake} \sim 5\%$. (For comparison, LHC b-tagging algorithms achieve $\epsilon \sim 70\%$, with a fake rate $\epsilon_{fake} \sim 1\%$.) It is evident from the performance curves that the ATLAS tagger outperforms the CMS tagger when high signal efficiency is required, while CMS does better at lower signal efficiency. Even the simple two-variable N-subjettiness tagger outperforms both CMS and ATLAS taggers by a notable margin, except at high signal efficiency, while adding the additional multivariate discrimination to the N-subjettiness tagger provides a significant improvement. Further updates in the BOOST 2011 workshop show that (1) being more precise about modeling QCD radiation at wide angles and (2) including the effects of finite detector resolution reduce typical efficiencies to $\epsilon \sim 40\%$, at a (QCD) background mistag rate in the range $\epsilon_{fake} \sim 2-8\%$
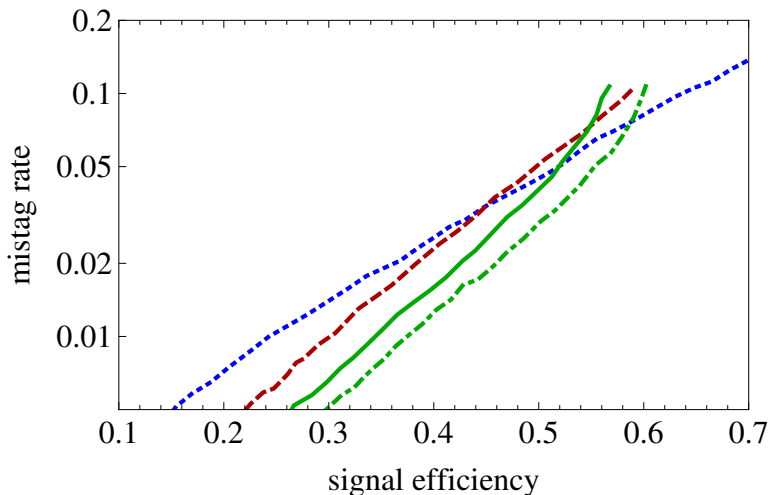
Figure 6: Top tagging performance curves, for tops with $200\,\text{GeV} < p_T < 800\,\text{GeV}$ in the BOOST 2010 reference samples for: ATLAS (blue, dotted); CMS (red, dashed); and N-subjettiness in both the simple (green, solid) and multivariate (green, dot-dashed) versions. Data from Refs. [15, 28].

depending on the tagger [42]. Incorporating finite detector resolution also tends to reduce (but not erase!) the relative advantage of N-subjettiness over the sequential decomposition-based taggers.

4.2 BSM searches with jet substructure

New physics produces jets with substructure when the kinematics are governed by a nontrivial hierarchy of scales. For the top examples we've been discussing, this hierarchy arises from the separation between the scale characterizing new physics and the electroweak scale:

$$\Lambda_{NP} \gg \Lambda_{EW} \gg \Lambda_{QCD}. \tag{4.43}$$

The little hierarchy problem results in a very strong motivation for developing tagging techniques for boosted SM objects. Besides the top tagging discussed in the previous subsection, much effort has also gone into tagging boosted W, Z, and H bosons arising from the decay of new TeV-scale particles[43, 44, 45, 46]. This is fortunate for theorists, as, once these techniques are put into use at experiments in one context, the barrier is much lower for their adaptation in other contexts where the theoretical motivation may not be so universal.

What other kinds of BSM physics are amenable to substructure analyses? To engender events with interesting substructure, some multi-tiered hierarchy of scales is required. We will enumerate an illustrative but far from exhaustive set of examples.

Supersymmetry is one example of a new physics sector which naturally can generate multiple scales. For example, if supersymmetry is broken at very high scales, RG effects will drive the colored superpartners much heavier than those superpartners with only EW charges. Thus, at the weak scale one could naturally expect $M_{\tilde{g}} \gg M_{\chi^0}$. In the presence of a large hierarchy between gluino and neutralino, the decay products of the neutralino would be collimated. Let us further suppose that the neutralino decays via the R-parity violating udd superpotential operator, so that $\chi^0 \to qqq$. Then gluino pair production would appear as a six-jet final state, where two of the jets are actually boosted neutralinos, containing interesting substructure [47]. The very large particle content of the MSSM can easily accommodate many possible hierarchies, with different theoretical origins; see for instance Ref. [48] for another of the many possibilities.

Another way to generate a hierarchy in a BSM sector is if the new physics sector contains a broken global symmetry, so that the scale $\Lambda^{(1)}$ characterizing the lightest states is set by the magnitude of the global symmetry breaking, rather than by the overall scale of the new sector, $\Lambda^{(2)} \gg \Lambda^{(1)}$. Thus consider, for example, a composite rho ρ_C, decaying into two pseudo-Nambu-Goldstone bosons π_C, which are stable within their own sector, and therefore must subsequently decay into SM objects [49].

Hidden valley models also have this kind of multi-scale structure. Here the hierarchy is between the mass of the mediator which connects the visible and hidden sectors and the mass scale of the light states in the hidden sector,

$$\Lambda_{med} \gg \Lambda_{NP} > \Lambda_{SM}. \tag{4.44}$$

The mediating particle might be a SM particle, in particular the H or Z, or a novel field such as a Z' [50] or the SM LSP [51]. Exotic Higgs decays to light particles also fall under this umbrella [52, 16, 53, 54, 55, 56].

More generally, thinking more broadly and flexibly about jets leads to new approaches to combinatorics and event reconstruction [57], and provides novel methods to distinguish QCD events from new physics. As challenging high-multiplicity and all-hadronic final states become a larger component of the LHC program, flexible and creative jet techniques will be critical to our ability to discover and interpret the physics. Jet algorithms themselves are still an evolving field! The anti-k_T algorithm was introduced only a few years ago. As the nature of the questions that we ask about jets evolves, so do the best jet algorithms to address these questions. There is still a lot of

room for new ideas!

5   Further Reading

References which were invaluable in the preparation of these lectures are the text *QCD and Collider Physics*, by Ellis, Stirling, and Webber [11], and the lecture notes "Toward Jetography" by Salam [58]. The proceedings of the BOOST 2010 and 2011 workshops [15, 42] are valuable resources for those looking for a quantitative survey of both theoretical and experimental progress in jet physics at the Tevatron and the LHC.

Acknowledgments

References

[1] G. F. Sterman and S. Weinberg, Phys. Rev. Lett. **39**, 1436 (1977).

[2] W. Bartel *et al.* [JADE Collaboration], Z. Phys. C **33**, 23 (1986).

[3] S. Bethke *et al.* [JADE Collaboration], Phys. Lett. B **213**, 235 (1988).

[4] S. Catani, Y. L. Dokshitzer, M. Olsson, G. Turnock and B. R. Webber, Phys. Lett. B **269**, 432 (1991).

[5] S. D. Ellis and D. E. Soper, Phys. Rev. D **48**, 3160 (1993) [hep-ph/9305266].

[6] S. Catani, Y. L. Dokshitzer, M. H. Seymour and B. R. Webber, Nucl. Phys. B **406**, 187 (1993).

[7] Y. L. Dokshitzer, G. D. Leder, S. Moretti and B. R. Webber, JHEP **9708**, 001 (1997) [hep-ph/9707323].

[8] M. Cacciari, G. P. Salam and G. Soyez, JHEP **0804**, 063 (2008) [arXiv:0802.1189 [hep-ph]].

[9] M. Cacciari and G. P. Salam, Phys. Lett. B **641**, 57 (2006) [hep-ph/0512210].

[10] J. M. Butterworth, A. R. Davison, M. Rubin and G. P. Salam, Phys. Rev. Lett. **100**, 242001 (2008) [arXiv:0802.2470 [hep-ph]].

[11] R. K. Ellis, W. J. Stirling, and B. R. Webber, *QCD and Collider Physics* (Cambridge Monographs on Particle Physics, Nuclear Physics and Cosmology, Cambridge University Press, Cambridge, UK, 2003).

[12] M. Dasgupta, L. Magnea and G. P. Salam, JHEP **0802**, 055 (2008) [arXiv:0712.3014 [hep-ph]].

[13] G. Aad *et al.* [ATLAS Collaboration], JHEP **1205**, 128 (2012) [arXiv:1203.4606 [hep-ex]].

[14] D. Krohn, J. Thaler and L. -T. Wang, JHEP **1002**, 084 (2010) [arXiv:0912.1342 [hep-ph]].

[15] A. Abdesselam, E. B. Kuutmann, U. Bitenc, G. Brooijmans, J. Butterworth, P. Bruckman de Renstrom, D. Buarque Franzosi and R. Buckingham *et al.*, Eur. Phys. J. C **71**, 1661 (2011) [arXiv:1012.5412 [hep-ph]].

[16] A. Falkowski, D. Krohn, L. -T. Wang, J. Shelton and A. Thalapillil, Phys. Rev. D **84**, 074022 (2011) [arXiv:1006.1650 [hep-ph]].

[17] S. D. Ellis, C. K. Vermilion and J. R. Walsh, Phys. Rev. D **80**, 051501 (2009) [arXiv:0903.5081 [hep-ph]].

[18] S. D. Ellis, C. K. Vermilion and J. R. Walsh, Phys. Rev. D **81**, 094023 (2010) [arXiv:0912.0033 [hep-ph]].

[19] D. E. Soper and M. Spannowsky, JHEP **1008**, 029 (2010) [arXiv:1005.0417 [hep-ph]].

[20] W. Skiba and D. Tucker-Smith, Phys. Rev. D **75**, 115010 (2007) [hep-ph/0701247].

[21] S. D. Ellis, C. K. Vermilion, J. R. Walsh, A. Hornig and C. Lee, JHEP **1011**, 101 (2010) [arXiv:1001.0014 [hep-ph]].

[22] G. Aad *et al.* [Atlas Collaboration], Phys. Rev. D **83**, 052003 (2011) [arXiv:1101.0070 [hep-ex]].

[23] J. Gallicchio and M. D. Schwartz, Phys. Rev. Lett. **107**, 172001 (2011) [arXiv:1106.3076 [hep-ph]].

[24] L. G. Almeida, S. J. Lee, G. Perez, G. F. Sterman, I. Sung and J. Virzi, Phys. Rev. D **79**, 074017 (2009) [arXiv:0807.0234 [hep-ph]].

[25] J. Thaler and L. -T. Wang, JHEP **0807**, 092 (2008) [arXiv:0806.0023 [hep-ph]].

[26] L. G. Almeida, S. J. Lee, G. Perez, G. Sterman and I. Sung, Phys. Rev. D **82**, 054034 (2010) [arXiv:1006.2035 [hep-ph]].

[27] J. Thaler and K. Van Tilburg, JHEP **1103**, 015 (2011) [arXiv:1011.2268 [hep-ph]].

[28] J. Thaler and K. Van Tilburg, JHEP **1202**, 093 (2012) [arXiv:1108.2701 [hep-ph]].

[29] I. W. Stewart, F. J. Tackmann and W. J. Waalewijn, Phys. Rev. Lett. **105**, 092002 (2010) [arXiv:1004.2489 [hep-ph]].

[30] J. Gallicchio and M. D. Schwartz, Phys. Rev. Lett. **105**, 022001 (2010) [arXiv:1001.5027 [hep-ph]].

[31] V. M. Abazov *et al.* [D0 Collaboration], Phys. Rev. D **83**, 092002 (2011) [arXiv:1101.0648 [hep-ex]].

[32] A. Hook, M. Jankowiak and J. G. Wacker, JHEP **1204**, 007 (2012) [arXiv:1102.1012 [hep-ph]].

[33] D. Curtin, R. Essig and B. Shuve, arXiv:1210.5523 [hep-ph].

[34] K. Rehermann and B. Tweedie, JHEP **1103**, 059 (2011) [arXiv:1007.2221 [hep-ph]].

[35] [ATLAS Collaboration], ATL-PHYS-PUB-2009-081, ATL-PHYS-PUB-2010-008.

[36] [CMS Collaboration], CMS-PAS-JME-09-001.

[37] D. E. Kaplan, K. Rehermann, M. D. Schwartz and B. Tweedie, Phys. Rev. Lett. **101**, 142001 (2008) [arXiv:0806.0848 [hep-ph]].

[38] G. Brooijmans, ATL-PHYS-CONF-2008-008, ATL-COM-PHYS-2008-001, Jan 2008.

[39] J. M. Butterworth, B. E. Cox and J. R. Forshaw, Phys. Rev. D **65**, 096014 (2002) [hep-ph/0201098].

[40] T. Plehn, G. P. Salam and M. Spannowsky, Phys. Rev. Lett. **104**, 111801 (2010) [arXiv:0910.5472 [hep-ph]].

[41] T. Plehn, M. Spannowsky, M. Takeuchi and D. Zerwas, JHEP **1010**, 078 (2010) [arXiv:1006.2833 [hep-ph]].

[42] A. Altheimer, S. Arora, L. Asquith, G. Brooijmans, J. Butterworth, M. Campanelli, B. Chapleau and A. E. Cholakian *et al.*, J. Phys. G **39**, 063001 (2012) [arXiv:1201.0008 [hep-ph]].

[43] G. D. Kribs, A. Martin, T. S. Roy and M. Spannowsky, Phys. Rev. D **81**, 111501 (2010) [arXiv:0912.4731 [hep-ph]].

[44] A. Katz, M. Son and B. Tweedie, JHEP **1103**, 011 (2011) [arXiv:1010.5253 [hep-ph]].

[45] Y. Cui, Z. Han and M. D. Schwartz, Phys. Rev. D **83**, 074023 (2011) [arXiv:1012.2077 [hep-ph]].

[46] M. Son, C. Spethmann and B. Tweedie, JHEP **1208**, 160 (2012) [arXiv:1204.0525 [hep-ph]].

[47] J. M. Butterworth, J. R. Ellis, A. R. Raklev and G. P. Salam, Phys. Rev. Lett. **103**, 241803 (2009) [arXiv:0906.0728 [hep-ph]].

[48] J. Fan, D. Krohn, P. Mosteiro, A. M. Thalapillil and L. -T. Wang, JHEP **1103**, 077 (2011) [arXiv:1102.0302 [hep-ph]].

[49] Y. Bai and J. Shelton, JHEP **1207**, 067 (2012) [arXiv:1107.3563 [hep-ph]].

[50] M. Baumgart, C. Cheung, J. T. Ruderman, L. -T. Wang and I. Yavin, JHEP **0904**, 014 (2009) [arXiv:0901.0283 [hep-ph]].

[51] C. Cheung, J. T. Ruderman, L. -T. Wang and I. Yavin, JHEP **1004**, 116 (2010) [arXiv:0909.0290 [hep-ph]].

[52] C. -R. Chen, M. M. Nojiri and W. Sreethawong, JHEP **1011**, 012 (2010) [arXiv:1006.1151 [hep-ph]].

[53] D. E. Kaplan and M. McEvoy, Phys. Rev. D **83**, 115004 (2011) [arXiv:1102.0704 [hep-ph]].

[54] C. Englert, T. S. Roy and M. Spannowsky, Phys. Rev. D **84**, 075026 (2011) [arXiv:1106.4545 [hep-ph]].

[55] I. Lewis and J. Schmitthenner, JHEP **1206**, 072 (2012) [arXiv:1203.5174 [hep-ph]].

[56] P. Draper and D. McKeen, Phys. Rev. D **85**, 115023 (2012) [arXiv:1204.1061 [hep-ph]].

[57] A. Hook, E. Izaguirre, M. Lisanti and J. G. Wacker, Phys. Rev. D **85**, 055029 (2012) [arXiv:1202.0558 [hep-ph]].

[58] G. P. Salam, Eur. Phys. J. C **67**, 637 (2010) [arXiv:0906.1833 [hep-ph]].